JOURNAL OF Materials CHEMISTRY

Vibrational and electronic spectroscopic properties of zirconia powders

Enrique Fernández López,[a] Vicente Sánchez Escribano,[a] Marta Panizza,[b] Maria M. Carnasciali[c,d] and Guido Busca*[b,d]

[a]*Departamento de Química Inorgánica, Facultad de Ciencias Químicas, P. de la Merced s/n 37008 Salamanca, Spain*
[b]*Dipartimento di Ingegneria Chimica e di Processo, Università di Genova, P.le J.F. Kennedy, I-16129 Genova, Italy. E-mail: icibusca@csita.unige.it; Fax: +39-010-3536028*
[c]*Dipartimento di Chimica e Chimica Industriale, Università di Genova, Via Dodecaneso 31, I-16146 Genova, Italy*
[d]*INFM, c/o Dipartimento di Fisica, Università di Genova, Via Dodecaneso 33, I-16146 Genova, Italy*

Received 25th January 2001, Accepted 27th April 2001
First published as an Advance Article on the web 6th June 2001

Ten zirconia powders have been characterized by XRD, FT-IR/FT-FIR and Raman skeletal spectroscopies and DR-UV electronic spectroscopy. The vibrational features of a yttria-stabilized cubic zirconia and of tetragonal, monoclinic and tetragonal+monoclinic pure zirconia mixtures have been discussed. Assignments for the vibrational features of cubic and tetragonal samples are proposed. The origin of very broad vibrational peaks in tetragonal zirconia is briefly addressed. The vibrational spectra provide evidence for the presence of trigonal oxide ions in the monoclinic phase only. The UV spectra show that monoclinic zirconia (where the coordination of zirconium is sevenfold) absorbs at lower energy than the cubic and tetragonal phases (where the coordination of zirconium is eightfold). However, it absorbs at higher energy than the perovskite $SrZrO_3$ where Zr adopts octahedral coordination. The origin of the shifts of the corresponding absorption edges is discussed.

Introduction

Zirconium dioxide is found in nature in small quantities as the mineral baddeleyite (monoclinic zirconia). It can also exist in tetragonal and cubic forms, both stable at higher temperature but stabilized by doping down to room temperature.

Zirconia is however a remarkable product of the inorganic chemical industry[1,2] as obtained by reduction of the mineral zircon ($ZrSiO_4$) with lime and coke. It can be used to form several kinds of mixed oxides used as refractories, abrasives, piezoelectric and capacitor materials, glasses and enamels. It is entirely non-toxic and allows slight non-stoichiometry.

Owing to its high melting point (>3000 K) zirconia ceramics (mostly stabilized with CaO or MgO) are utilized in furnace construction, for the manufacture of melting crucibles, and in the steel industry for continuous casting nozzles. When stabilized in the tetragonal form TZP ceramics (tetragonal zirconia polycrystals) are obtained, with very high mechanical strength. Owing to its low neutron capture cross section, Hf-free zirconia is used as a neutron reflector in nuclear reactor technology. When stabilized with yttria, zirconia exhibits unusually high ionic conductivity, and so is used as a solid electrolyte in fuel cells and in oxygen sensor devices, *e.g.* for car catalytic converters.

Owing to its total transparency to visible light and its high refractive index (2.1–2.2), zirconia is a good white pigment, and a good opacifier.[3] Zirconia is also produced as a coating for titania white pigments, to limit UV excitation of titania itself so limiting its photocatalytic activity in converting organic paint binders.

Zirconia is also a relevant material in adsorption and catalysis. It exhibits rather basic character and is active in hydrogenation/dehydrogenation as well as in hydration/dehydration reactions. Additionally, zirconia has been proposed as a promising support for hydro-desulfurization processes[4] and for the selective catalytic reduction of NO_x by ammonia (SCR[5]). When sulfated[6] or combined with tungsten oxide[7] zirconia is an extremely active catalyst in converting hydrocarbons at low temperature.

In previous papers we have pointed out that the electronic properties of the supports are relevant in activating the performances of oxide–supported oxide[8] and sulfide catalysts.[9] This may also be the case for zirconia based catalysts active in hydrocarbon conversion.[10,11] On the other hand, optical spectroscopy of zirconias is relevant also with respect to their use as coatings and as pigments. We present here our results about the spectroscopic properties of a number of different zirconia powders in the range of their vibrational and electronic transitions.

Experimental

Some data on the samples under study are summarized in Table 1. Some samples were commercial ones while others were home made. Sample B was prepared by reduction of zirconyl nitrate with tartaric acid *via* a procedure similar to that described in ref. 12. Samples E and I were prepared by precipitation from zirconyl nitrate as reported in ref. 13. Samples F and J were prepared by calcination of a precipitate from zirconium(IV) acetate with aa aqueous solution of ammonium carbonate. Chemical analyses showed that sample A contained 13.25% (w/w) Y_2O_3 as a stabilizing agent while samples F and J contained 0.5% (w/w) TiO_2 as an impurity.

Powder X-ray diffraction spectra were recorded on a Philips

Table 1 Summary of the samples under study

Name	Origin	Calcination T/K	Specific surface/$m^2\ g^{-1}$	V_m (%)	Crystal size[a]/nm
A	Tosoh	As received	4	Cubic	55 c
B	Reactive reduction of the nitrate	As such	47	0	17 t
C	B calcined	1273	40	16	17 t
D	Degussa	As received	50	19	16 t/20 m
E	Precipitated from Zr nitrate (ref. 13)	723	94	55	20 t/8 m
F	Precipitated from Zr acetate	1073	11	80	20 t
G	Janssen	As received	70	94	17 m
H	Thann et Mulhouse	As received	15	97	27 m
I	Precipitated from Zr nitrate (ref. 13)	1273	18	98	27 m
J	F, calcined	1473	<4	100	44 m

[a]Calculated for the cubic phase (c), tetragonal phase (t) or monoclinic phase (m).

PW1710/PW1729 diffractometer (CoK_α radiation, 30 kV, 30 mA).

The FT-IR spectra were recorded using a Nicolet Magna 750 Fourier Transform instrument. For the region above 400 cm^{-1} a KBr beam splitter was used with a DTGS detector. For the FIR region (600–50 cm^{-1}) a "solid substrate" beam splitter and a DTGS polyethylene detector were used. KBr pressed disks (IR region) and polyethylene pressed disks (FIR region) were used.

The FT-Raman spectra were recorded using a Bruker FTS100 (Nd–YAG laser). The laser Raman spectra were recorded using a Renishaw SYSTEM 2000 (He–Ne laser, 633 nm).

Diffuse reflectance spectra in the range 2500–200 nm were obtained with a Jasco V-570 spectrophotometer at room temperature. The BET surface areas were measured with a conventional volumetric instrument by nitrogen adsorption at liquid nitrogen temperature.

Results and discussion

1. XRD data

In Fig. 1 the XRD patterns of the zirconia samples under study in the region 2θ 30–40° are reported. Sample A, which is a commercial sample stabilized with yttria, is cubic as expected. No trace of other phases are detected. The XRD pattern is fully compatible with that expected for a fluorite-type structure with space group $Fm3m$ (225) and $Z=4$ (ICSD no. 27-0997). Most of the other samples show XRD patterns which are mixtures of tetragonal zirconia (space group $P4_2/nmc$ (137) and $Z=2$, ICSD no. 42-1164) and monoclinic zirconia (baddeleyite, space group $P2_1/a$ (14) and $Z=4$, ICSD no. 37-1484). Actually sample B is pure tetragonal zirconia and sample J is purely monoclinic. According to the procedure of Toraya *et al.*[14] the respective Bragg reflections of the tetragonal [(111)t] and of the monoclinic form [($\bar{1}$11)m and (111)m] of zirconia were fitted and separated. From the resulting intensity values, the volume fraction (V_m) of the monoclinic phase was calculated, as summarized in Table 1. Mean particle sizes were evaluated using the Debye–Scherrer formula,[15] as also reported in Table 1.

2. FT-IR/FT-FIR and Raman skeletal spectra

The IR/FIR and the FT-Raman spectra of our zirconia preparations in the skeletal regions are reported in Figs. 2 and 3 respectively. It is well known that vibrational spectroscopies are very useful techniques for the determination of the crystal phase for zirconia. The irreducible representations for the optical modes for the three zirconia polymorphs, as obtained by applying the correlation method,[16] are summarized in Table 2. It is evident that the spectra for the cubic sample are expected to be very simple, with only one fundamental mode active in Raman and another one only active in IR. The active modes increase markedly upon lowering the symmetry of the structure, *i.e.* by going from cubic to tetragonal and then to monoclinic zirconia. Owing to the very different spectra

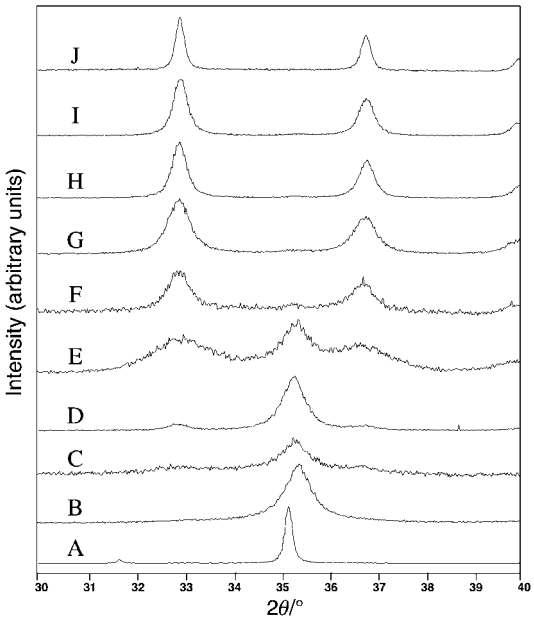

Fig. 1 XRD patterns of zirconia samples.

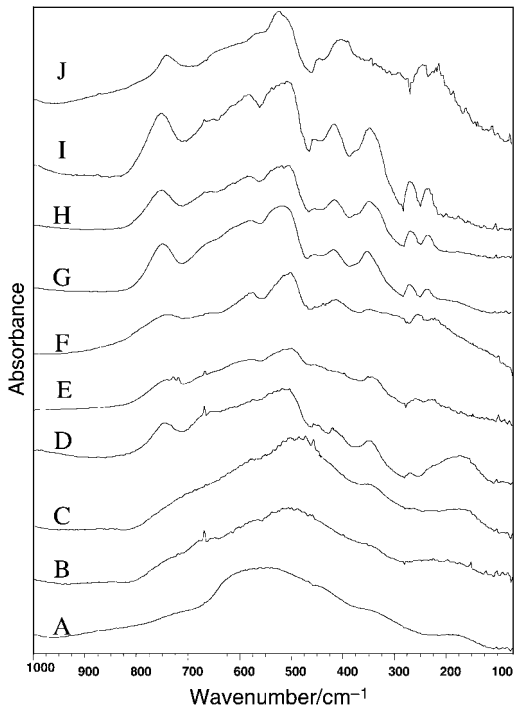

Fig. 2 FT-IR-FIR spectra of zirconia samples.

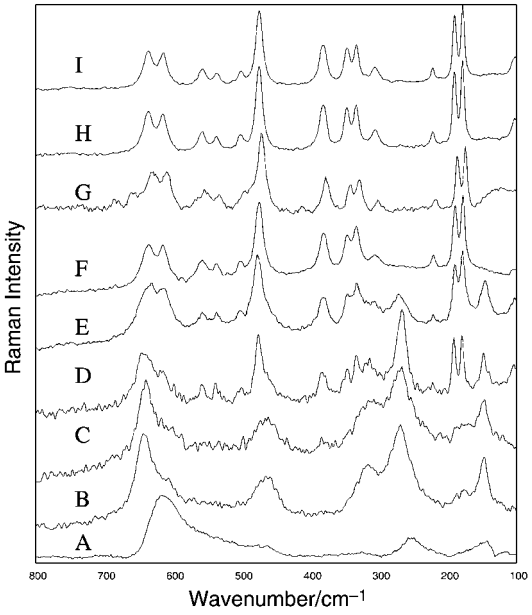

Fig. 3 FT-Raman spectra of zirconia samples.

expected, vibrational spectroscopy has been used widely in the past to characterize zirconia preparations.[17–22] Actually, Raman spectra are generally well defined and very useful for characterization, while IR spectra are more difficult to apply. Additionally, some discrepancies can be seen in earlier reports. Moreover, the interpretation of the spectra is largely incomplete.

In agreement with the above, spectra of increasing complexity are obtained for cubic, tetragonal and monoclinic zirconia.

Table 2 Evaluation of the number of IR and R active modes of zirconia polymorphs[a]

Cubic, space group $Fm3m \equiv O_h^5$ (no. 225), $Z=4$, $Z_B=1$

Atom	N_B	Site symmetry	
Zr	1	O_h	F_{1u}
O	2	T_d	$F_{1u}+F_{2g}$
Total			$2\ F_{1u}+F_{2g}$
Acoustic			F_{1u}
Optical		R active	F_{2g} (1 peak expected)
		IR active	F_{1u} (1 band expected)

Tetragonal, space group $P4_2/nmc \equiv D_{4h}^{15}$ (no. 137), $Z=Z_B=2$

Atom	N_B	Site symmetry	
Zr	2	D_{2d}	$B_{1g}+E_g+A_{2u}+E_u$
O	4	C_{2v}	$A_{1g}+B_{1g}+2\ E_g+A_{2u}+B_{2u}+2\ E_u$
Total			$A_{1g}+2\ B_{1g}+3\ E_g+2\ A_{2u}+B_{2u}+3\ E_u$
Acoustic			$A_{2u}+E_u$
Optical		R active	$A_{1g}+2\ B_{1g}+3\ E_g$ (6 peaks expected)
		IR active	$A_{2u}+2\ E_u$ (3 bands expected)
		inactive	B_{2u}

Monoclinic, space group $P2_1/c \equiv C_{2h}^5$ (no. 14), $Z=Z_B=4$

Atom	N_B	Site symmetry	
Zr	4	C_1	$3\ A_g+3\ B_g+3\ A_u+3\ B_u$
O (I)	4	C_1	$3\ A_g+3\ B_g+3\ A_u+3\ B_u$
O (II)	4	C_1	$3\ A_g+3\ B_g+3\ A_u+3\ B_u$
Total			$9\ A_g+9\ B_g+9\ A_u+9\ B_u$
Acoustic			$A_u+2\ B_u$
Optical		R active	$9\ A_g+9\ B_g$ (18 peaks expected)
		IR active	$8\ A_u+7\ B_u$ (15 bands expected)

[a] Z_B and N_B are the number of formulae units and number of atoms, respectively, in the smallest Bravais cell.

As for the stabilized cubic phase, sample A, one only Raman active mode and one IR active mode are expected. Actually, a major peak is observed in the Raman spectrum at 616 cm^{-1}, which should be assigned to the triply degenerate F_{2g} fundamental. The breadth of this peak is anomalous, and this has been assigned to a "one phonon density of states", owing to structural disorder associated with oxygen vacancies in such Y-doped samples.[19] Interestingly, this mode arises from the symmetric motions of the oxygen atoms only. Owing to the high symmetry of the tetrahedra which surround oxygen, this mode arises from the three equivalent motions of oxygen on the three axes (F_2 symmetry for the T_d site symmetry). Owing to the presence of two oxygen atoms in the smallest Bravais cell and to the O_h factor group, this mode splits into one symmetric component (F_{2g}) and one asymmetric component (F_{1u}). This mode corresponds to coupled Zr–O–Zr asymmetric stretching and deformation modes. However, its symmetric component (Raman active) can also be regarded as a symmetric O–Zr–O stretching.

The IR spectrum of sample A shows a broad main maximum at 530 cm^{-1}, with a pronounced shoulder near 620 cm^{-1} and a weaker one near 725 cm^{-1}. The IR spectrum of our stabilized cubic sample A is similar to the spectra published in the literature for corresponding samples: although the main maximum is evident at 480 cm^{-1}, these authors assign a pronounced shoulder near 625 cm^{-1} to the IR active fundamental mode.[15,19] In contrast, it seems reasonable to assign the main maximum we observe at 530 cm^{-1} to the triply degenerate F_{1u} mode (transverse mode, TO) and the weaker component near 725 cm^{-1} to the corresponding longitudinal mode (LO). In fact this mode is generated by the movements of both Zr and O atoms, which couple giving rise to the triply degenerate acoustic mode. Thus, this mode is expected to fall at lower frequency with respect to the Raman active fundamental, also because of the involvement of Zr ions. However, the position of the absorption suggests that the movements of oxygen atoms dominate in determining this mode. Thus, it can be assigned essentially to the asymmetric motions of oxygen atoms with respect to the center of symmetry. This mode is consequently an asymmetric O–Zr–O stretching. The shoulder near 620 cm^{-1} may be due to the Raman active mode activated in IR as a result of the decrease of symmetry arising from the partial substitution of Zr with Y.

Interestingly, the Raman spectrum of sample A shows additional peaks which are clearly associated with tetragonal zirconia impurities not detected by XRD. This shows that Raman spectroscopy probably detects small domains of tetragonal zirconia which are not detected by XRD.

According to its structural properties, the tetragonal zirconia phase is expected to give rise to 6 Raman peaks and 3 IR bands, which should also undergo TO–LO splitting. The Raman spectra of samples B and C clearly show the 6 peaks which are associated with Raman active fundamentals. We detect these peaks at 639 cm^{-1}, 604 cm^{-1} (shoulder), 463 cm^{-1}, 314 cm^{-1}, 268 cm^{-1} and 145 cm^{-1}, for samples B and C. In both cases, further weaker peaks (in particular at 170–190 cm^{-1}) correspond to peaks of the monoclinic phase, so they are probably attributable to monoclinic zirconia impurities. Also in these cases Raman seems to be more sensitive than XRD in detecting these impurities. The IR spectra of B and C are still very broad with one dominant maximum now around 500 nm. As shown also by Hirata *et al.*,[21] the spectrum is similar to that of the cubic phase, but without the component near 620 cm^{-1}. Also in our case (like for the samples described by Hirata[20] and by Phillippi and Mazdiyasni[17]) the breadth of the IR absorption is similar for cubic and tetragonal samples, while the breadth of the Raman peak of the tetragonal phase is not smaller than that of the cubic phase. We note, however, that while our sample A is a commercial stabilized yttria-containing cubic zirconia, our tetragonal samples B and C are

Table 3 Correlation of the vibrational modes of cubic and tetragonal zirconia

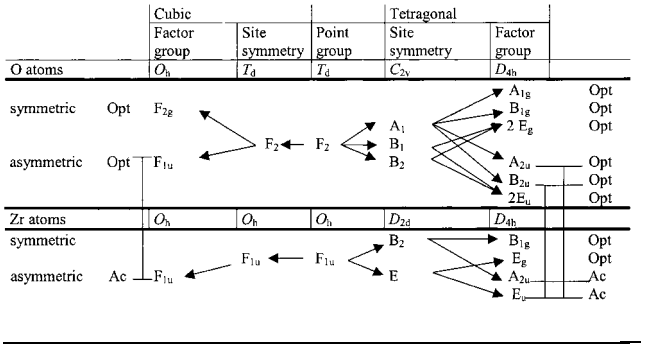

virtually free from dopants, so that the breadth of the vibrational features in the case of our tetragonal samples cannot be due to disorder arising from doping. However, it could be associated with the small crystal size, as reported in Table 1.

To our knowledge the positions of the four IR active components of tetragonal zirconia have never been defined with certainty. The inspection of our spectra suggests that a band is probably located near 160 cm^{-1} with another one near 575 cm^{-1}. To gain some more definite information about this we attempted a correlation between the forecasted modes for cubic and tetragonal zirconia (Table 3).

The smallest Bravais cell of tetragonal zirconia contains four oxygen atoms, in comparison with the two of the cubic phase. Additionally, the tetrahedra surrounding oxygen are deformed, *i.e.* they are expanded in the *c* direction (C_{2v} site symmetry). So every movement of oxygen atoms undergoes threefold splitting ($A_1+B_1+B_2$ in the C_{2v} site symmetry). The movements of the four oxygen atoms combine giving rise to four non-degenerate modes and four doubly degenerate modes, four of which are IR active and four Raman active.

The A_1 motion takes the character of a symmetric Zr–O–Zr stretching mode coupled to an "in-plane" bending mode. In contrast, the B_1 and B_2 modes take the character of an asymmetric Zr–O–Zr stretching mode coupled with a rocking mode. In agreement with this, according to the literature,[19] the highest frequency Raman mode is E_g (asymmetric Zr–O–Zr stretching mode arising from the fully symmetric coupling of the B_1 and B_2 modes, 639 cm^{-1}) with a shoulder which is A_{1g} (symmetric Zr–O–Zr stretching mode arising from the fully symmetric coupling of the A_1 modes, 604 cm^{-1}). The partially symmetric coupling of the A_1 modes would give rise to the B_{1g} mode detected in Raman at 314 cm^{-1}, while the partially symmetric coupling of the B_1 and B_2 modes should give rise to the E_g mode detected in Raman at 463 cm^{-1}. The lowest frequency modes (268 cm^{-1}, E_g, and 145 cm^{-1}, B_{1g}) can be essentially assigned to movements of Zr ions.

According to the origin of the Raman peaks of tetragonal zirconia, discussed here, we can assign the apparent IR band near 160 cm^{-1} to a mode dominated by the movement of Zr ions, E_u. Two bands associated with the movements of oxide ions, both undergoing TO–LO splitting, are expected in the range 400–650 cm^{-1}. This is the cause of the poor resolution of the bands in this region, as well as their intrinsic breadth. In any case we expect an IR active mode in the range 600–650 cm^{-1} (asymmetrically coupled asymmetric Zr–O–Zr stretching, E_u), and a mode arising from the symmetric Zr–O–Zr stretchings in the region 400–500 cm^{-1} ($A_{2u}+E_u$).

The IR and Raman spectra of monoclinic zirconia (samples G, H, I and J) are evidently even more complex than those of tetragonal zirconia. Also the IR spectrum exhibits a number of well defined bands. The Raman spectrum shows at least 16 peaks, and one pronounced shoulder, with respect to the 18 fundamentals which are expected. The highest frequency Raman peak is, however, very weak at 755 cm^{-1} and the question arises whether it is a fundamental or a harmonic mode.

The IR spectrum shows at least 12 components with at least 2 pronounced shoulders. Again we are near to the number of expected IR active modes, *i.e.* 15. A typical feature for the spectrum of monoclinic zirconia is the strong band at 770 cm^{-1}, which is far higher in frequency than the main features for the other zirconia polymorphs.

The structure of monoclinic zirconia actually exhibits a definite structural difference compared with the tetragonal and cubic phases. In monoclinic zirconia in fact the coordination of zirconium is sevenfold; in parallel (and this should have a more evident effect on the vibrational spectra) half of the oxygen atoms have planar trigonal coordination, although with three different Zr–O bond lengths.[23] The other half (located in a different crystallographic position although with the same site symmetry C_1) lie in a very distorted tetrahedral coordination.

We can suppose that the movements arising from tetrahedrally coordinated oxygen atoms occur in similar positions in tetragonal and monoclinic zirconia. In contrast, we expect additional bands (6 Raman peaks and 5 or 6 IR bands) due to the trigonal oxide ions, in the spectrum of monoclinic zirconia. This implies negligible coupling between the movements of tetrahedral and trigonal oxide atoms, which is obviously an approximation. Owing to the lower symmetry of the ZrO_7 polyhedra and of the Zr_4O "tetrahedra", additional splitting is expected.

The movements of oxygen atoms in OM_3 triangles give rise to an asymmetric stretching which is expected to lie at higher frequencies than the corresponding stretching modes of OM_4 tetrahedra. Obviously, owing to the presence of four trigonal oxygen atoms in the smallest Bravais cell, this mode should give rise to four components, two of which are IR active and two Raman active. On the other hand this mode is intrinsically associated with a large change in the dipole moment and to a small change in polarizability. It seems consequently reasonable to assign the weak Raman peak at 755 cm^{-1} and the strong IR band at 780 cm^{-1} to the R and IR active components of this mode.

A more complete but very tentative assignment of the modes of monoclinic zirconia is possible. We limit ourselves here to emphasising that the presence of trigonal oxide ions is very probably responsible for vibrational features at distinctly higher frequencies for monoclinic than for tetragonal and cubic phases. Raman spectroscopy also indicates the presence of impurities in sample G by small features in the region 650–700 cm^{-1}.

An anomalous Raman spectrum is found for sample J. For this reason, we analyzed it with a laser Raman microscope. The sample shows, under the Raman microscope, clear heterogenity (Fig. 4). The Raman spectrum of the "white" particles fully

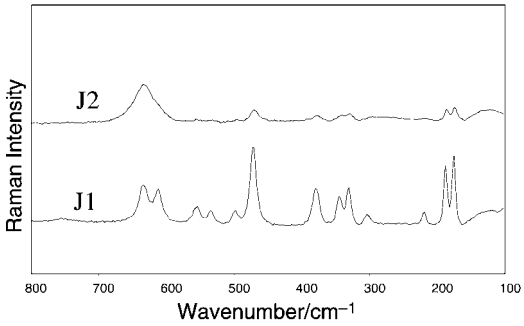

Fig. 4 Laser micro-Raman spectra of the sample J: J1 white particles, J2 pale yellow particles.

corresponds to that of the "predominantly" monoclinic samples. In contrast, some particles have a "pale yellow" aspect. Analysis of these particles indicates a very strong peak located at 634 cm^{-1}, and possibly a broad peak centered near 280 cm^{-1}, with a further peak near 120 cm^{-1}, in addition to the features of monoclinic zirconia. These features may be due to a cubic phase, possibly with a tetragonal phase also present. The presence of such an inhomogeneity suggests that the TiO_2 impurities present in this sample are distributed inhomogeneously and stabilize, after calcination at 1473 K, the cubic phase in some particles. The more pure zirconia particles retain the monoclinic structure.

3. Diffuse reflectance UV-vis spectra

Electronic spectra of the perovskite-type compounds $SrTiO_3$ and $SrZrO_3$, in which Ti and Zr exhibit octahedral coordination, and of $SrCO_3$ are reported in Fig. 5, for comparison. According to the d^0 configuration of the Ti^{4+} and Zr^{4+} ions (as well as of Sr^{2+}), no features characteristic of d–d transitions are displayed in the visible region (above 400 nm), and absorption edges appearing at higher energies (in the UV region) are attributed to charge transfer transitions from the valence band, having mainly O (2p) character, to the conduction band, having mainly 3d or 4d character, of Ti or Zr, respectively. The blue shift in the $SrZrO_3$ spectrum with respect to $SrTiO_3$ is in accord with the more difficult reducibility of Zr^{4+} relative to Ti^{4+}.[24] On the other hand we note that the spectrum of $SrZrO_3$ shows two well defined edges near 220 and 265 nm, and a further tail extending to 300–340 nm. A splitting of the O (2p)→Zr (4d) CT transition is expected because of the t_g–e_g splitting of the d orbitals in an octahedral environment. Comparison of the spectra in Fig. 5 supports the assignment of the absorption in the region above 230 nm to the O (2p)→Zr (4d) CT transition, while the edge below 230 nm should be associated with the O (2p)→Sr (4d) CT transitions.

Thus, the spectra in Fig. 5 allow us to determine the typical position of the CT transition associated with tetravalent Zr in octahedral coordination to be located in the range 250–350 nm and that, for isostructural compounds, tetravalent Zr species absorb at lower wavelength than tetravalent Ti species. This is relevant because of the several studies published concerning the UV spectra of Ti^{4+} species in oxide matrices.

The DR-UV spectra of the zirconia samples are shown in Fig. 6. Two of them, F and J, exhibit an anomalous aspect with a continuous absorption in the UV range, which is very likely to be due to the presence of TiO_2 impurities. The Raman spectrum of the J oxide varied significantly as a function of the point of the sample upon which the laser beam was focused (see Fig. 4), albeit previously it was necessary to perform a careful examination of the surface morphology (by means of electronic microscopy) in order to distinguish heterogeneous areas which were also worthy of analysis. In contrast, DR-UV-VIS spectroscopy is an immediate (and extremely sensitive) technique for the detection of such impurities in zirconium oxide.

The other spectra in Fig. 6 are in good agreement with those previously reported for zirconia[10] and show an intense absorption edge below 230 nm with a maximum located between 205 and 210 nm. In samples with low V_m values (*i.e.* for mixtures of tetragonal and monoclinic phases with a definite predominance of the tetragonal one) as well as for the cubic sample, an absorption tail extends up to about 240 nm, whereas in those where the monoclinic polymorph is predominant ($V_m > 0.5$) a second component arises at higher wavelengths. This component possesses comparable intensity with that for the practically monophasic monoclinic samples I and K.

These data strongly support the idea that eight-coordinate tetravalent Zr species (like those of cubic and tetragonal zirconia) are responsible for the absorption in the range 200–210 nm, while seven-coordinate Zr species (like those of monoclinic zirconia) are responsible for a split absorption with an additional component at 240 nm (*i.e.* at lower energy). As shown in Fig. 5, octahedral Zr species give rise to absorption at even lower energy.

All of the observed bands can be reasonably assigned to the allowed O^{2-} (2p)→Zr^{4+} (4d) charge transfer transitions.[25] For comparison, we note the blue shift with respect to the spectra of the polymorphs of titania, anatase and rutile, given in ref. 26, where, however, Ti is in octahedral coordination. Moreover, the decrease in the wavelength of the bands is also related (provided that bonding is primarily ionic) to the increase of the coordination number of the transition metal from 6 (for both anatase and rutile) to 7 or 8 (for zirconia polymorphs).

A qualitative interpretation of the UV spectra of zirconia can be given on the basis of the Crystal Field Theory which, in spite of its simplicity, is an accurate model for systems in which interelectronic repulsion need not be considered, and often gives rise to the same results as the more powerful Molecular Orbital Theory.[27]

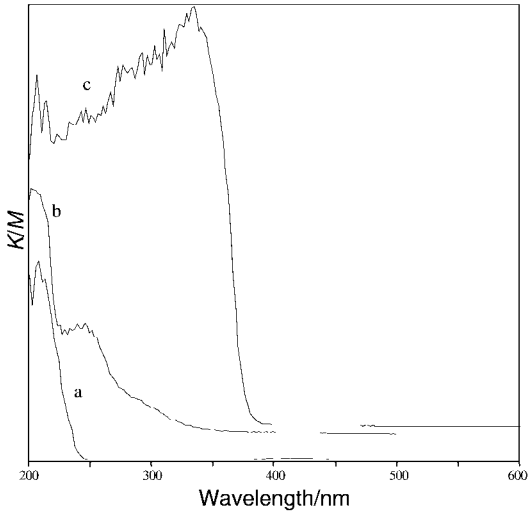

Fig. 5 DR-UV spectra of strontium carbonate (a), strontium zirconate (b) and strontium titanate (c).

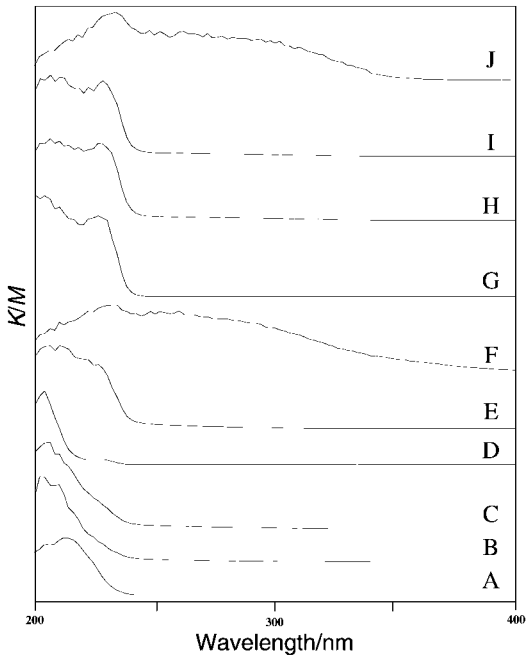

Fig. 6 DR-UV spectra of zirconia samples.

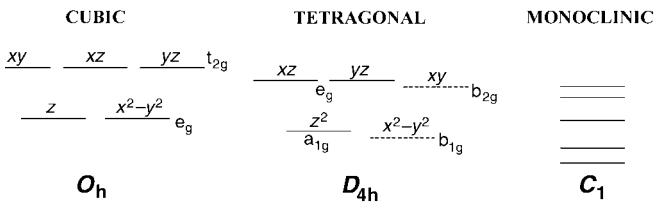

Fig. 7 Crystal field splitting diagrams for cubic, tetragonal and monoclinic polymorphs of zirconia. Dashed lines in the representation of tetragonal zirconia indicate a theoretical splitting of d-levels which is not evident in the electronic spectra. For monoclinic zirconia, only the complete splitting of d orbitals is shown without any assignment. Diagrams are not to scale.

Thus, a cube with 8 O^{2-} at the vertices is chosen as a representation of the 8-fold coordination of the Zr^{4+} ion (symmetry group O_h) in cubic zirconia. The electrostatic interaction between the 4d orbitals of Zr^{4+} (degenerate in spherical perturbation) with the surrounding environment of negative charges gives rise to the splitting of the former into the more stable e_g set, which points towards the centre of the faces of the cube, and the t_{2g} set, directed to the middle of the sides and consequently, closer to the O^{2-} ions (see Fig. 7 for the representation of the orbital splitting in zirconia polymorphs). The absorption edge observed in the electronic spectrum for cubic zirconia (A) can then be assigned to an electronic transition from the valence band (having approximately the energy of the 2p shell of oxygen) to the e_g level of the Zr^{4+} ion.

The elongation of the coordination polyhedron along the z axis gives rise to tetragonal zirconia, in which Zr^{4+} has D_{4h} symmetry. This transition should result from a formal point of view in the decrease of energy of the d orbitals located in the horizontal plane, namely $d_{x^2-y^2}$ and d_{xy}, from which the effective withdrawal of negative charge becomes greater. Accordingly, the splitting of the lower e_g level into e_{1g} and e_{1g}, and of the higher t_{2g} level into b_{2g} and b_g is expected, as depicted in Fig. 7, and in the electronic spectra of the predominantly tetragonal samples (B, C and D) is detectable above $\lambda = 200$ nm.

The removal of one oxygen from the coordination environment of zirconium gives rise to the monoclinic distortion of the unit cell of zirconia; the coordination index of Zr^{4+} diminishes to 7 and it acquires non-axial symmetry C_1. This change must result in the total loss of degeneracy of the d levels, greater for those 'out of plane' (previously closer to the negative point charges) and, as a consequence, in the electronic spectra of samples E–I a second component develops at higher wavelengths upon increasing the monoclinic phase content. Hence, the observed bands can be tentatively ascribed, in decreasing order of wavelength, to $O^{2-}(2p) \rightarrow Zr^{4+}(4d_{x^2-y^2})$ and $O^{2-}(2p) \rightarrow Zr^{4+}4d(_{z^2})$ charge transfer transitions. Anyway, it seems reasonable to state that the occurrence of the second component in the spectra of zirconia is related to the further splitting of the energy levels of the conduction band with the reduction of symmetry of the unit cell. Furthermore, the slight red shift of the first maximum in the spectra of samples E–I may be due to the decrease of electrostatic repulsion between O^{2-} anions and d orbitals of Zr^{4+} for the seven-fold coordination of the metal (when one oxygen is removed from the surrounding environment). Finally, it is worthwhile to note that the absorption tail following the main bands decays notably for monoclinic zirconia, which may account for its assignment to a partially overlapped $O^{2-}(2p) \rightarrow Zr^{4+}(A_{1g})$ transition in tetragonal zirconia.

According to this discussion, the observed trend of the position of the absorption onset for Zr oxides which is (in terms of energy): cubic $ZrO_2 \sim$ tetragonal $ZrO_2 >$ monoclinic $ZrO_2 > SrZrO_3$, is associated with the coordination number of the Zr^{4+} ion (*i.e.* $8 > 7 > 6$) and to the extent of splitting of the non-hybrid 4d orbitals of Zr^{4+}.

Conclusions

The work presented here allowed a discussion of the optical properties of the different zirconia phases in the IR and UV visible regions, and of the Raman scattering behavior. Vibrational spectroscopies have confirmed phase analysis of zirconia preparations to be made and in particular Raman spectroscopy is found to be even more sensitive than XRD for the detection of phase impurities.

A more complete analysis of the vibrational spectra of zirconia samples has been attempted here. In particular the IR spectra of monoclinic zirconia allow the detection of trigonal oxide ions as a typical feature of this structure.

The UV spectra show that monoclinic zirconia absorbs at lower energy than tetragonal and cubic zirconia. This indicates that monoclinic zirconia can be preferentially used to cut out more UV light, *e.g.* for protecting titania powders or other UV absorbing materials.

This different electronic behavior can also explain the different behavior of tetragonal *versus* monoclinic zirconia, *e.g.* in producing (when sulfated) highly active catalysts for hydrocarbon conversion. In fact the paraffin skeletal isomerization reaction is though to involve redox cycles that are certainly sensitive to the electronic properties of the support.

Raman and UV spectroscopy allow one also to detect TiO_2 impurities in some samples, which escape XRD analysis.

Acknowledgements

E.F.L. acknowledges a grant from Junta de Castilla y León. M.M.C. and G.B. acknowledge funding from INFM.

References

1 W. Buchner, R. Schliebs, G. Winter and K. H. Buchel, *Industrial Inorganic Chemistry*, VCH, Weinheim, 1989, p. 442.
2 R. Nielsen, in *Ullmann's Enciclopedia of Industrial Chemistry*, ed. B. Elvers and S. Hawkins, 5th edn., vol. A28, p. 543.
3 P. A. Lewis, *Pigment Handbook*, Wiley, New York, 1988, vol. I, p. 67.
4 D. Hamon, M. Vrinat, M. Breysse, B. Durand, F. Beauchesne and T. des Courieres, *Bull. Soc. Chim. Belg.*, 1991, **108**, 933.
5 V. Indovina, M. Occhiuzzi, P. Ciambelli, D. Sannino, G. Ghiotti and F. Prinetto, in *11th Intenational Congress on Catal.—40th Anniversary*, ed. J. W. Hightower, W. N. Delgass, E. Iglesia and A. T Bell, *Stud. Surf. Sci. Catal*, 1996, **101**, 691.
6 K. Arata, *Adv. Catal.*, 1990, **37**, 165.
7 D. G. Barton, S. L. Soled, G. D. Meitzer, G. A. Fuentes and E. Iglesia, *J. Catal.*, 1999, **57**, 181.
8 L. J. Alemany, L. Lietti, N. Ferlazzo, P. Forzatti, G. Busca, E. Giamello and F. Bregani, *J. Catal.*, 1995, **155**, 117.
9 J. Ramirez, L. Cedeño and G. Busca, *J. Catal.*, 1999, **59**, 184.
10 A. Gutiérrez Alejandre, J. Ramírez and G. Busca, *Catal. Lett.*, 1998, **56**, 30.
11 A. Gutierrez-Alejandre, P. Castillo, J. Ramirez, G. Ramis and G. Busca, *Appl. Catal. A: General*, 2001, in press.
12 F. Abbattista, S. Delmastro, G. Gozzelino, D. Mazza, M. Vallino, G. Busca, V. Lorenzelli and G. Ramis, *J. Catal.*, 1989, **117**, 42.
13 M. Daturi, A. Cremona, F. Milella, G. Busca and E. Vogna, *J. Eur. Ceram. Soc.*, 1998, **18**, 1079.
14 H. Toraya, M. Yoshimura and S. Somiya, *J. Am. Ceram. Soc.*, 1984, **67**, C-119.
15 A. J. West, *Solid state chemistry and its applications*, Wiley, Chichester, p. 174.
16 W. G. Fateley, F. R. Dollish, N. T. McDevitt and F. F. Bentley, *Infarared and Raman Selection Rules for Molecular and Lattice Vibrations*, Wiley, New York, 1972.
17 C. M. Phillippi and K. S. Mazdiyasni, *J. Am. Ceram. Soc.*, 1971, **54**, 254.
18 D. P. C. Thackeray, *Spectrochim. Acta, Part A*, 1974, **30**, 549.
19 C. H. Perry, D. W. Liu and R. P. Ingel, *J. Am. Ceram. Soc.*, 1985, **68**, C184.

20 T. Hirata, H. Zhu, T. Furubayashi and I. Nakatani, *J. Am. Ceram. Soc.*, 1993, **76**, 1361.
21 T. Hirata, E. Asari and M. Kitajima, *J. Solid State Chem.*, 1994, **110**, 201.
22 C. G. Kontoyannis and G. Carountsos, *J. Am. Ceram. Soc.*, 1994, **77**, 2191.
23 A. Gualtieri, P. Norby, J. Hanson and J. Hriljac, *J. Appl. Crystallogr.*, 1996, **29**, 707.
24 C. K. Jørgensen, *Absorption Spectra and Chemical Bonding in Complexes*, Pergamon Press, London, 1962, p. 146.
25 D. Sutton, *Electronic Spectra of Transition Metal Complexes*, McGraw Hill, London, 1968, p. 14.
26 H. Bevan, S. V. Dawes and R. A. Ford, *Spectrochim. Acta*, 1958, **13**, 43.
27 A. B. P. Lever, *Inorganic Electronic Spectroscopy*, Elsevier, Amsterdam, 2nd edn., 1984, p. 129.